Carbon Nanotubes

DOI: 10.1002/anie.201007832

Coaxially Stacked Coronene Columns inside Single-Walled Carbon Nanotubes**

Toshiya Okazaki, Yoko Iizumi, Shingo Okubo, Hiromichi Kataura, Zheng Liu, Kazu Suenaga, Yoshio Tahara, Masako Yudasaka, Susumu Okada, and Sumio Iijima*

One of the most interesting features of molecular materials is the fact that their physical properties change with the arrangement of the molecules as well as with the properties of the molecules themselves. Self-organization is an efficient pathway through which organic molecules assemble to form well-ordered nanometer-scale objects that are hardly synthesized by conventional chemical reactions. In these systems, two or more molecules are held together and are assembled by means of intermolecular (noncovalent) bonding such as ion–dipole or dipole–dipole interactions, hydrogen bonding, hydrophobic interactions, or π–π stacking. Such molecular self-organization and recognition processes are among the most practical and effective means to facilitate a "bottom-up" approach in nanotechnology. In general, however, fabrication of well-defined organic nanowires or other types of one-dimensional (1D) nanostructures with controllable size and morphology is not as far advanced as for their inorganic counterparts.[1,2]

[*] Prof. T. Okazaki, Y. Iizumi, Dr. S. Okubo, Dr. Z. Liu, Dr. K. Suenaga, Y. Tahara, Dr. M. Yudasaka, Prof. S. Iijima
Nanotube Research Center, National Institute of Advanced Industrial Science and Technology (AIST)
Tsukuba 305-8565 (Japan)
Fax: (+81) 29-861-6241
E-mail: toshi.okazaki@aist.go.jp
Prof. T. Okazaki
PRESTO (Japan) Science and Technology Agency (JST)
4-1-8 Honcho, Kawaguchi 332-0012 (Japan)
Prof. T. Okazaki, Y. Iizumi
Department of Chemistry, University of Tsukuba
1-1-1 Tennodai, Tsukuba 305-8577 (Japan)
Dr. H. Kataura
Nanosystem Research Institute, AIST
Tsukuba 305-8562 (Japan)
Prof. S. Okada
Institute of Physics and Center for Computational Sciences
University of Tsukuba, Tsukuba 305-8577 (Japan)
and
Japan Science and Technology Agency, CREST
Tokyo 102-0075 (Japan)

[**] We thank Drs. N. Kishi (Nagoya Institute of Technology) and T. Saito (AIST) for their experimental assistance in the synthesis of coronenes@SWCNTs and spectroscopic measurements. We also thank Drs. M. Tange, A. Furube (AIST), Y. Hayamizu (University of Washington), and Y. Kitahama (Kwansei Gakuin Univ.) for helpful discussions. Partial support by Grants-in-Aid from MEXT (Japan) is acknowledged by T.O. (no21685017) and by Z.L. and K.S. (no19054017).

Supporting information for this article is available on the WWW under http://dx.doi.org/10.1002/anie.201007832.

Single-walled carbon nanotubes (SWCNTs) can offer a suitable interior space for the accommodation of molecules.[3–5] Nanostructures produced by the incorporation of such molecules into SWCNTs are expected to exhibit several superior features. For example, because the diameter of SWCNTs can be adjusted to the size of the molecules, well-ordered molecular arrangements more than a micrometer in length can be easily produced. The synthesized molecular arrangements are also expected to be strong and flexible under mechanical strain because the nanotube templates sustain the structure. Furthermore, the already synthesized nanostructures are isolated from reactive species by the tube wall, which leads to the superior durability of the encapsulated molecules.[6]

Herein we demonstrate such a 1D SWCNT-templated nanostructure using planar π-conjugated molecules (coronenes). Encapsulated coronenes form nano-scale columns in a way that differs from 3D solid coronenes, thus resulting in electronic and optical properties peculiar to the 1D structure. The production of well-ordered molecular assemblies in SWCNTs can be expected to inspire novel approaches for the synthesis of low-dimensional molecular materials with unique physical properties.

The self-organized 1D structure of coronenes inside SWCNTs (coronenes@SWCNTs) was achieved through vapor-phase doping (Figure 1).[7] Coronene confinement in nanometer spaces produces a characteristic columnar structure. Figure 1b,d and Figure S2a (see the Supporting Information) show high-resolution TEM (HRTEM) images of the coronene columns inside SWCNTs; coronene molecules are positioned along the tube axis at almost regular intervals. The formation of the columnar structure is due to two dominant factors: π–π stacking between coronenes and the interaction between the encapsulated coronene and the host SWCNT. In the monoclinic crystal, coronenes have an interplanar distance of 0.34 nm with a tilt angle of about 46° relative to the stacking axis.[8] On the other hand, within SWCNTs, statistical analysis of the HRTEM images shows that the distance between the molecular planes is 0.35 ± 0.03 nm (Figure S2b) and the angle between the molecular plane and the tube axis (θ) is approximately 77° (Figure S2c, 1c). Although the interplanar distances are identical between 1D and solid coronenes within the experimental error, a substantial difference is observed for the tilt angle.

The observed structure that involves coronene columns was supported by total energy calculations for zig-zag (n, 0) SWCNTs. Figure 1e shows the stabilization energy (ΔE) of coronenes inside SWCNTs as a function of tube diameter (d), where the molecular plane of coronenes was set to be

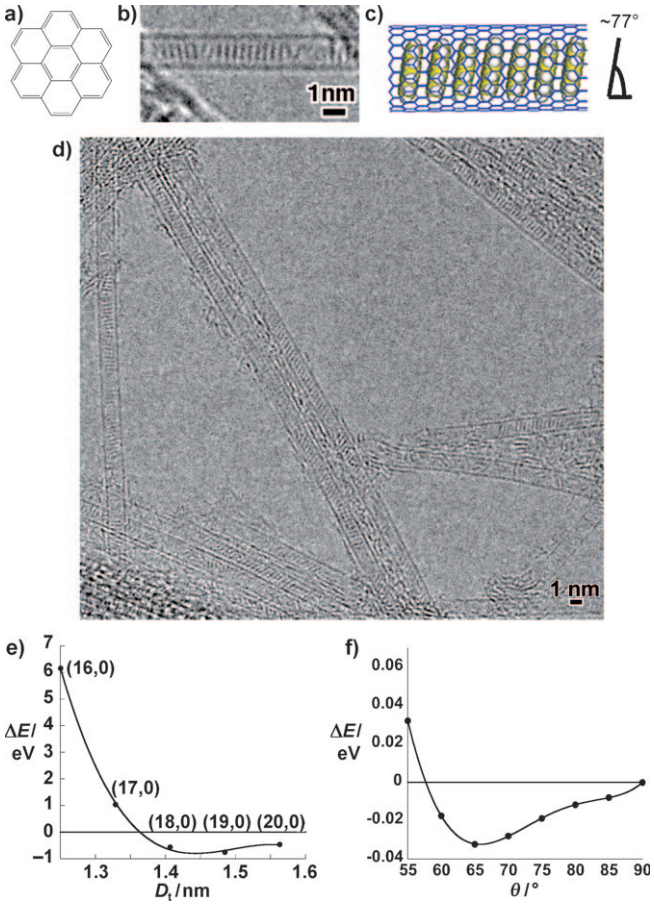

Figure 1. a) Molecular structure of coronene. b), d) HRTEM images of SWCNTs encapsulating coronenes. c) Schematic illustration of SWCNTs encapsulating coronenes. e) Theoretically calculated results for the stabilization energy (ΔE) of coronenes inside SWCNTs as a function of tube diameter for (n, 0) tubes. f) Calculated ΔE of coronenes@(19, 0) SWCNTs as a function of the tilt angle of the encapsulated coronenes. Note that ΔE at $\theta = 90°$ is set to be 0.

perpendicular to the tube axis. DFT calculations show that the encapsulation is exothermic for SWCNTs with $d > 1.36$ nm, with the most favorable diameter being around 1.45 nm ($\Delta E \approx -0.8$ eV). Figure 1 f shows the tilt angle dependence of ΔE for (19, 0) SWCNTs ($d \approx 1.51$ nm). The optimum angle of approximately 65° is a result of the balance between the coronene–coronene and coronene–SWCNT interactions. This value is similar to the observed tilt angle ($\theta \approx 77°$). Note that the interval between coronene molecules was set to 0.42 nm in this calculation to match the unit-cell length of (19, 0) tubes. This length is somewhat longer than the observed value (0.35 nm). Shorter inter-planar distances should increase the tilt angle so as to stack the coronene planes more efficiently. Consequently, the optimum angle would increase, and more closely approximate the observed angle ($\theta \approx 77°$).

The Raman spectra of the coronenes@SWCNTs and original SWCNTs excited at 514.5 nm are shown in Figure 2 and S3. The vibrational modes that originate from the coronenes are observed in a broad frequency region (Figure S3, Table S1). As a result of the D_{6h} symmetry of coronene, the E_{2g} and A_{1g} vibrations are Raman-active.[9,10]

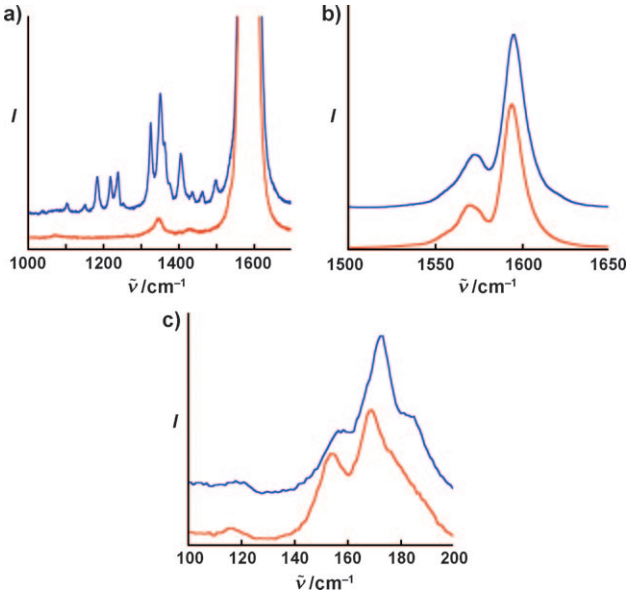

Figure 2. a) Raman spectra of the coronenes@SWCNTs (blue) and original SWCNTs (red) excited at 514.5 nm. b) G-bands and c) RBM of the coronenes@SWCNTs and original SWCNTs.

The most intense bands of the coronene modes are observed at 1325 and 1350 cm^{-1} (Figure 2 a), which can be assigned to in-plane A_{1g} modes.[9,10] The observed vibrational frequencies are shifted by approximately 24 and approximately 16 cm^{-1} to higher wavenumbers, respectively, relative to those of the solid-state coronenes.[10] The interaction between coronenes and SWCNTs may induce vibrational softening in the coronene columns.

The G-band and the radial breathing mode (RBM) of the coronenes@SWCNTs are shown in Figure 2 b and c. It is well known that the vibrational frequency of the G-band is highly sensitive to the charge transfer between the encapsulated molecules and SWCNTs.[11] Such a shift is not observed for coronenes@SWCNTs (less than 1 cm^{-1}), thus indicating the absence of apparent charge transfer between the coronenes and SWCNTs. As observed in other SWCNTs with encapsulated molecules,[6,12] the spectral shape of the RBM mode also changes when coronenes are encapsulated; variation of the RBM ensures high-yield filling of the SWCNTs.

Normally, luminescence from encapsulated molecules is severely quenched by the surrounding SWCNTs because of the effective energy transfer from the encapsulated molecules to SWCNTs.[13–15] However, inside the SWCNTs, coronenes exhibit visible fluorescence under UV light (Figure 3 a). Figure 3 b and S7 show the fluorescence spectra observed from coronenes@SWCNTs, together with the reference spectrum of coronene in hexane solution. The lack of the excitation wavelength dependence ensures that the observed fluorescence is composed of a single spectrum (Figure S7). The emission spectrum of coronene in hexane (Figure 3 b) shows a highly structured band, with several vibrational origins in the 400–550 nm spectral region—a region that corresponds to the S_0–S_1 transition band.[16,17] On the other hand, the fluorescence from coronenes in SWCNTs exhibits characteristic features that can be attributed to the well-

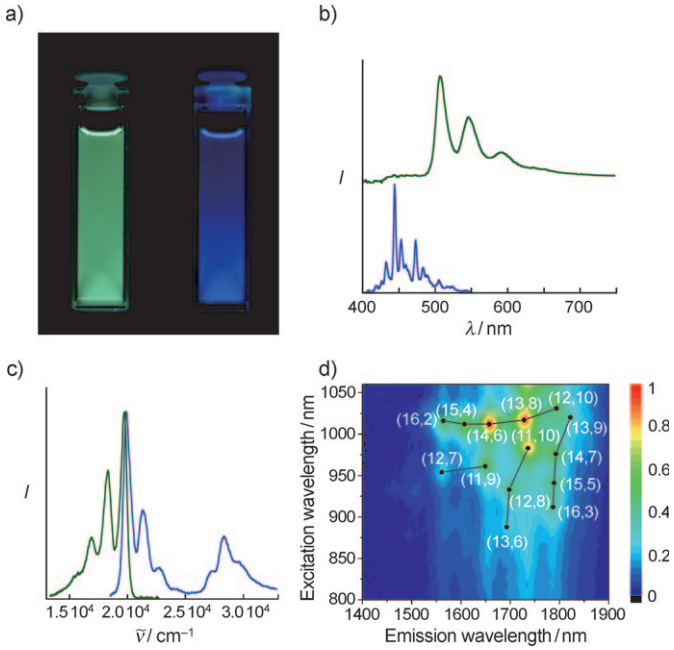

Figure 3. a) Photograph of the fluorescence from coronenes@SWCNTs in SDBS micelle solution (left) and coronene in *n*-hexane solution (right) under UV lamp irradiation ($\lambda_{ex} = 356$ nm). b) Fluorescence spectra of coronenes@SWCNTs in SDBS–D_2O (green) and coronene in *n*-hexane (blue) under 350 nm excitation. c) Excitation spectrum of coronenes@SWCNTs in SDBS–D_2O probed at 550 nm (blue) and the fluorescence spectrum (green). d) PL intensity contour plot of coronenes@SWCNTs in SDBS-D_2O.

defined 1D arrangement of coronene molecules (Figure 3b). For example, even though the spectral shape becomes broader, vibrational progression is still clearly observable in the fluorescence spectrum of coronene columns. The fact that the clear vibronics are seen in the coronenes@SWCNTs spectrum is inconsistent with the common assignment of the spectrum to an excimer or a self-trapped exciton.[18–21] This observation suggests that the coronenes inside SWCNTs preserve their molecular characters, in contrast to the 3D solids of coronenes. Furthermore, the observed fluorescence spectrum is considerably red-shifted (ca. 500 nm) with respect to the molecular coronenes (ca. 426 nm, Figure 3b)[16] and the coronene crystal (ca. 432 nm).[18,19] Although the detailed mechanism is unclear, it is hypothesized that stronger coronene–coronene interactions in the 1D arrangement and/or generally larger exciton-binding energies in quasi-1D systems[22,23] might be relevant to the observed large red-shift.

The fluorescence quantum yield of coronenes@SWCNTs was 0.014 at an excitation wavelength of 350 nm. The ratio of the absorbance of the encapsulated coronenes to that of SWCNTs is roughly estimated to be 1:10 at 350 nm. This result leads to a quantum yield of approximately 0.15 for the encapsulated coronenes while that of coronene in ethanol was 0.23.[24] The smaller quantum yield of coronenes@SWCNTs may be a result of the energy transfer from coronenes to the host SWCNTs (see also the Supporting Information).

The excitation spectrum of the coronenes@SWCNTs is also shown in Figure 3c. The intense and structured profiles with peaks around 20000–24000 cm^{-1} and 27000–30000 cm^{-1} correspond to the S_0–S_1 and S_0–S_2 transition bands, respectively. The clear mirror-image symmetry between the excitation and fluorescence spectra with a small Stokes shift (ca. 120 cm^{-1}) is indicative of a small structural relaxation in the excited state of the coronenes.

The two-dimensional infrared photoluminescence (PL) contour plot of coronenes@SWCNTs in a micelle solution is shown in Figure 3d. The fact that bright PL peaks can be observed from the host SWCNTs rules out a strong charge-transfer reaction between SWCNTs and the encapsulated coronenes.[11] The observed PL peak positions were shifted from those of the original SWCNTs (Figure S4a). The dependence of these PL peak shifts on the diameter indicates that the interaction between coronenes and SWCNTs can be explained by weak intermolecular forces (see the Supporting Information).[7,25] Note that the PL peak positions of SWCNTs, the diameters of which are less than approximately 1.32 nm, remain unchanged. The value of 1.32 nm is consistent with the theoretically predicted limit of coronene encapsulation (Figure 1e).

The 1D coronene columns in SWCNTs show unique electronic and spectroscopic properties that are very distinct from those of the coronene molecule in solution and in 3D solids. This observation indicates that SWCNTs can possess fairly unique nanospaces that can be used for molecular nanostructures. The practical value of SWCNT-templated 1D structures may also prove to be extremely high; one can readily conceive of applications for molecular electronics and photonic devices. For example, emission of visible light from the encapsulated coronenes could influence the design of materials for optoelectronic devices.[15,26] This hybrid material also has potential for biological imaging because SWCNTs can encapsulate imaging probes while their outer surfaces can be functionalized.[27] Figure 4 shows confocal fluorescence

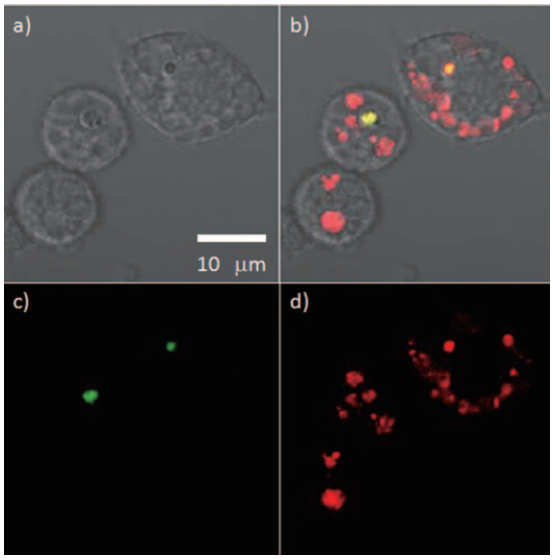

Figure 4. Confocal microscope images of murine macrophage cell line RAW 264.7 after incubation with coronenes@SWCNTs wrapped in DSPE-mPEG. a) Differential interference contrast (DIC) image. b) Combined DIC and fluorescence images. Fluorescence images obtained from c) coronenes@SWCNTs and d) lysosomal markers (excitation wavelength = 488 nm, detection wavelength > 510 nm).

microscopy images of the murine macrophage cell line RAW264.7 treated with coronenes@SWCNTs wrapped in 1,2-distearoyl-phosphatidylethanolamine-methyl-polyethyleneglycol (DSPE-mPEG, M_w 5000). The green color corresponds to the emission from coronenes inside SWCNTs (Figure 4c) while the red fluorescence is emitted from lysosomal markers (Figure 4d). Apparently, the green spots overlap with some of the red spots, thus appearing as yellow or orange spots (Figure 4b). These observations indicate that DSPE-mPEG-wrapped coronenes@SWCNTs are localized in lysosomes (Figure 4b,d). Successful internalization of coronenes@SWCNTs by phagocytosis suggests that this material can be targeted to particular cells or tumours by proper functionalization of the tube wall.[27–29] Advantageously, multimodal bioimaging probes can also be achieved by the codoping of molecules[30] with different functionalities, such as fluorescent molecules and MRI contrast agents, into SWCNTs. Such "smart" and targeted multimodal agents could become the next-generation probes for imaging technologies.

Experimental Section

Synthesis of coronenes@SWCNTs: A self-organized 1D structure of coronene molecules inside SWCNTs (coronenes@SWCNTs) was obtained through vapor-phase doping.[7] Briefly, purified SWCNTs were heated at 500 °C for 30 min to open their caps, and then sealed with coronenes in a quartz tube under vacuum (ca. 1×10^{-4} Pa). Upon heating at approximately 450 °C, coronene molecules sublimate individually and migrate into SWCNTs (ca. 24 h). The synthesized coronenes@SWCNTs were washed with toluene and annealed at approximately 300 °C under vacuum to remove excess coronenes that adhere to the outer wall (see the Supporting Information for more details).

Aqueous micellar solutions of coronenes@SWCNTs for absorption, fluorescence, excitation, and PL measurements were prepared according to a procedure similar to that described by Bachilo et al.[31] Typically, coronenes@SWCNTs (ca. 1 mg) were dispersed for 10 min in D_2O (ca. 20 mL) that contains 1 wt % of dodecylbenzene sulfonate (SDBS), using a 200 W homogenizer (SONICS VCX500) equipped with a titanium alloy tip (TI-6Al-4V). Each solution was then centrifuged at 123000 g for 2.5 h (HITACHI CP 100MX), after which the supernatant was used for testing.

TEM analyses: The HRTEM images were taken using a JEOL-2010F equipped with a CEOS postspecimen spherical aberration corrector (C_s corrector) operated at 120 kV. For the HRTEM investigations, samples were dispersed in methanol by ultrasonication. The specimens were kept at ambient temperature during the observation. A Gatan 894 CCD camera was used for digital recording of the HRTEM images. Damage to the specimen by the electron beam was reduced as much as possible (the beam density was about 10000 electrons/(nm^2 s) or 0.16 C cm^{-2}). The HRTEM images were recorded under slightly under-focused conditions to enhance the contrast of coronenes with respect to the SWCNT graphene network.

Raman spectroscopy: Raman measurements were performed using a JASCO NR2100 system with an excitation wavelength of 514.5 nm. Spectra were obtained by integration for 240 s. A silicon wafer was used to calibrate the spectra and "buckypaper" made of coronenes@SWCNTs was used for measurements.

Fluorescence and excitation spectroscopy: Fluorescence spectra from coronene columns in SWCNTs were measured with a Horiba Spex Fluorolog 3–2 TRIAX system. The fluorescence spectra of two control samples (coronene dispersed in 1wt % SDBS solution in D_2O and a mechanical mixture of SWCNTs and coronene dispersed in 1wt % SDBS solution in D_2O) are shown in Figure S5. Excitation spectra were measured with a Hitachi U4500 spectrometer. Aqueous micellar solutions of coronenes@SWCNTs were used for measurements. The fluorescence quantum yield of coronenes@SWCNTs was measured using a Hamamatsu model C9920-02 absolute PL quantum yield measurement system.

Near-infrared photoluminescence spectroscopy: PL mapping was performed with a Shimadzu NIR-PL system utilizing an IR-enhanced InGaAs detector (Princeton Instruments OMA-V2.2) for detection and a tunable Ti-sapphire laser (Spectra Physics 3900S) for excitation. The slit width for emission was 10 nm. Typical scan steps were 5 and 2 nm for excitation and emission, respectively. The raw data were corrected for wavelength-dependent instrumental factors and excitation laser intensities. Aqueous micellar solutions of coronenes@SWCNTs were used for measurements.

Theoretical calculations: The electronic structure calculations and geometry optimizations were performed using local-density approximation in DFT with the plane wave basis set and the norm-conserving pseudopotential.[32] The stabilization energy (ΔE) of coronenes inside zig-zag (n, 0) SWCNTs (Figure 1e,f) was calculated for the following reaction,

$$(n, 0)\ \text{SWCNTs} + \text{coronenes} \rightarrow \text{coronenes@SWCNTs} - \Delta E. \quad (1)$$

Note that the tube diameters in Figure 1e were calculated by using the C–C bond length of 0.142 nm.

In vitro cell imaging: Bioconjugated aqueous micellar solutions of coronenes@SWCNTs for absorption, excitation, and PL measurements were prepared according to a procedure similar to that described by Welsher et al.[33] Briefly, we first debundled and dispersed coronenes@SWCNTs in water by SDB as described above. The suspension was ultracentrifuged at 123000 g for 1 h to remove any bundles. 1,2-Distearoyl-phosphatidylethanolamine-methyl-polyethyleneglycol conjugate-5000 (DSPE-mPEG, M_w 5000, 1 mg mL^{-1}) was added to the supernatant solution and the mixture was bath-sonicated for 3 min to fully dissolve the DSPE-mPEG. The solution was then dialyzed by using a 3500 molecular weight cut-off membrane over 5 days with the water changed several times a day. This process slowly displaced the DSPE-mPEG from the SDBS. We measured the absorption spectrum of the displaced water to check the residual concentration of SDBS. After 5 days, more than 89 % of the SDBS was displaced.

The murine macrophage cell line RAW264.7 (ECACC) was cultured in RPMI1640 medium supplemented with 10 % fetal bovine serum, penicillin, and streptomycin at 37 °C in 5 % CO_2/air with 95 % relative humidity. The cells were placed in 35 mm glass-bottom culture dishes (IWAKI) and grown overnight. Subsequently, coronenes@SWCNTs dispersed in DSPE-mPEG in water (200 μL) were added to the culture medium (2 mL) and further incubated for 24 h. After incubation, following medium removal and washing with phosphate-buffered saline, lysosomes were labeled with Lysotracker Red (Molecular Probes; 50 ng mL^{-1}) for 20 min. Cells were imaged using a Zeiss LSM 5 Pascal laser-scanning microscope (Carl Zeiss) with a ×100 oil immersion lens.

Received: December 13, 2010
Revised: February 25, 2011
Published online: March 23, 2011

Keywords: fluorescence · molecular imaging probe · nanostructures · nanotubes · self-assembly

[1] L. Zang, Y. Che, J. S. Moore, *Acc. Chem. Res.* **2008**, *41*, 1596–1608.
[2] L. C. Palmer, S. I. Stupp, *Acc. Chem. Res.* **2008**, *41*, 1674–1684.

[3] B. W. Smith, M. Monthioux, D. E. Luzzi, *Nature* **1998**, *396*, 323 – 324.
[4] M. Monthioux, *Carbon* **2002**, *40*, 1809 – 1823.
[5] D. A. Britz, A. N. Khlobystov, *Chem. Soc. Rev.* **2006**, *35*, 637 – 659 .
[6] K. Yanagi, Y. Miyata, H. Kataura, *Adv. Mater.* **2006**, *18*, 437 – 441.
[7] S. Okubo, T. Okazaki, N. Kishi, S.-K. Joung, T. Nakanishi, S. Okada, S. Iijima, *J. Phys. Chem. C* **2009**, *113*, 571 – 575.
[8] J. M. Robertson, J. G. White, *J. Chem. Soc.* **1945**, 607 – 617.
[9] K. Ohno, *J. Chem. Phys.* **1991**, *95*, 5524 – 5538.
[10] C. Castiglioni, C. Mapelli, F. Negri, G. Zerbi, *J. Chem. Phys.* **2001**, *114*, 963 – 974.
[11] L. Kavan, L. Dunsch, *ChemPhysChem* **2007**, *8*, 974 – 998.
[12] S.-K. Joung, T. Okazaki, N. Kishi, S. Okada, S. Bandow, S. Iijima, *Phys. Rev. Lett.* **2009**, *103*, 027403.
[13] K. Yanagi, K. Iakoubovskii, S. Kazaoui, N. Minami, Y. Maniwa, Y. Miyata, H. Kataura, *Phys. Rev. B* **2006**, *74*, 155420.
[14] K. Yanagi, K. Iakoubovskii, H. Matsui, H. Matsuzaki, H. Okamoto, Y. Miyata, Y. Maniwa, S. Kazaoui, N. Minami, H. Kataura, *J. Am. Chem. Soc.* **2007**, *129*, 4992 – 4997.
[15] K. Yanagi, H. Kataura, *Nat. Photonics* **2010**, *4*, 200 – 201.
[16] K. Ohno, T. Kajiwara, H. Inokuchi, *Bull. Chem. Soc. Jpn.* **1972**, *45*, 996 – 1004.
[17] T. Itoh, *J. Mol. Spectrosc.* **2008**, *252*, 115 – 120.
[18] A. H. Matsui, K. Mizuno, *J. Phys. D* **1993**, *26*, B242 – B244.
[19] T. Yamamoto, S. Nakatani, T. Nakamura, K. Mizuno, A. H. Matsui, Y. Akahama, H. Kawamura, *Chem. Phys.* **1994**, *184*, 247 – 254.
[20] T. Seko, K. Ogura, Y. Kawakami, H. Sugino, H. Toyotama, J. Tanaka, *Chem. Phys. Lett.* **1998**, *291*, 438 – 444.
[21] Y. Chen, J. Luo, X. X. Zhu, *J. Phys. Chem. B* **2008**, *112*, 3402 – 3409.
[22] T. Hasegawa, Y. Iwasa, H. Sunamura, T. Koda, Y. Tokura, H. Tachibana, M. Matsumoto, S. Abe, *Phys. Rev. Lett.* **1992**, *69*, 668 – 671.
[23] F. Wang, G. Dukovic, L. E. Brus, T. F. Heinz, *Science* **2005**, *308*, 838 – 841.
[24] A. R. Horrocks, F. Wilkinson, *Proc. R. Soc. London Ser. A* **1968**, *306*, 257 – 273.
[25] T. Okazaki, S. Okubo, T. Nakanishi, S.-K. Joung, T. Saito, M. Otani, S. Okada, S. Bandow S. Iijima, *J. Am. Chem. Soc.* **2008**, *130*, 4122 – 4128.
[26] M. A. Loi, J. Gao, F. Cordella, P. Blondeau, E. Menna, B. Bártová, C. Hébert, S. Lazar, G. A. Botton, M. Milko, C. Ambrosch-Draxl, *Adv. Mater.* **2010**, *22*, 1635 – 1639.
[27] S. Y. Hong, G. Tobias, K. T. Al-Jamal, B. Ballesteros, H. Ali-Boucetta, S. Lozano-Perez, P. D. Nellist, R. B. Sim, C. Finucane, S. J. Mather, M. L. H. Green, K. Kostarelos, B. G. Davis, *Nat. Mater.* **2010**, *9*, 485 – 490.
[28] N. W. Shi Kam, M. O'Connell, J. A. Wisdom, H. Dai, *Proc. Natl. Acad. Sci. USA* **2005**, *102*, 11600 – 11605.
[29] Z. Liu, W. Cai, L. He, N. Nakayama, K. Chen, X. Sun, X. Chen, H. Dai, *Nat. Nanotechnol.* **2007**, *2*, 47 – 52.
[30] K. Suenaga, Y. Sato, Z. Liu, H. Kataura, T. Okazaki, K. Kimoto, H. Sawada, T. Sasaki, K. Omoto, T. Tomita, T. Kaneyama, Y. Kondo, *Nat. Chem.* **2009**, *1*, 415 – 418.
[31] S. M. Bachilo, M. S. Strano, C. Kittrell, R. H. Hauge, R. E. Smalley, R. B. Weisman, *Science* **2002**, *298*, 2361 – 2366.
[32] M. Otani, S. Okada, A. Oshiyama, *Phys. Rev. B* **2003**, *68*, 125424.
[33] K. Welsher, Z. Liu, S. P. Sherlock, J. T. Robinson, Z. Chen, D. Daranciang, H. Dai, *Nat. Nanotechnol.* **2009**, *4*, 773 – 780.

